



SCIREA Journal of Electrical Engineering

<https://www.scirea.org/journal/DEE>

March 9, 2020

Volume 5, Issue 1, February 2020

Control of Two-Section 3D Printed Tele-operated Wire-Driven Continuum Robot Arm

Azamat Yeshmukhametov^{1,5,*}, Koichi Koganezawa², Askar Seidakhmet³, Yoshio Yamamoto⁴

¹School of Science and Technology, Tokai University, Hiratsuka, Japan

²Department of Robotics and Engineering Tools of Automation, Satbayev University, Almaty, Kazakhstan

³Department Applied Mechanics and CAD Engineering, Satbayev University, Almaty, Kazakhstan

⁴Department of Mechanical Engineering, Tokai University, Hiratsuka, Japan

⁵Department of Precision Engineering, Tokai University, Hiratsuka, Japan

*yeshmukhametov.coba@gmail.com

Abstract

In the last couple of decades, wire-driven mechanisms getting more attention in robotics and medical instruments. The wire-driven actuation system is one of the effective ways of force transmission in the distance. In continuum robots, a wire-driven mechanism plays a crucial role in robot control. Likewise, power transmission in a range allows us to locate motors in the base and improve robot design and dexterity features as well. However, a wire-driven mechanism cannot provide stiffness to the robot structure, which can negatively affect the robot's end-effector position. Therefore, many scholars and engineers contributing various types of continuum robot's backbone design to provide necessary rigidity to the robot

backbone during the work. Also, wire-driven mechanisms have a problem with tension control. Tendon actuated robots demand additional mechanisms to compensate for lost tension during the motion as well. So, the investigation will cover a novel pretension mechanism system to avoid wire slack and escape from the pulleys. The novelty of this research is proposed by robot kinematics and a new robot control strategy.

This research will describe a continuum robot backbone design and robot control, moreover, based on proposed robot design, forward kinematics, and control architecture of the robot.

Keywords: *Continuum robot, wire-driven, 3d printed, robot design, control, kinematics.*

1. Introduction

Attention to the continuum manipulators dramatically increased in the last couple of decades. One of the main reasons is a reaching ability in the unstructured and confined space, because of inherited flexible features of the backbone [1]. Therefore, continuum manipulator finds more application in rescue operations and minimally invasive surgery as well.

In continuum manipulators, the backbone plays a crucial role, so it holds all robot structure and routes cables or actuators. By the backbone design of the continuum, robots could be divided into three categories: *discrete hyper-redundant*, *hard continuum robot*, and a *soft continuum robot arm*. The *discrete hyper-redundant* continuum robot backbone consists of universal or ball joints and mostly supports by springs. Hyper-redundant continuum robots bend only in joints, and the segment length always keeps constant. Moreover, primarily hyper-redundant robot arms drive by wire [2,28,29]. Secondly, *hard continuum* robots backbone made of an elastic material such as spring or rubber. In some cases backbone could be made of magnet discs [3,27]. One of the main differences between hard continuum robots from a hyper-redundant robot is a bending feature. Hard continuum robot arm could bend in any segment and could be driven by wire and magnetic repulsion. Hard continuum manipulators recommended itself as a useful tool for minimally invasive surgery. *Soft continuum* manipulators are made of rubber and silicon materials. Mostly soft manipulator drives by fluid (pneumo) or dielectric elastomer [9], (Table 1).

By the continuum robots actuating system, it divides into three groups: wire-driven, fluid-driven (hydro or pneumo) actuation system, and dielectric elastomer system. The most

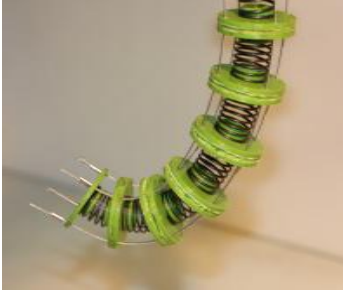
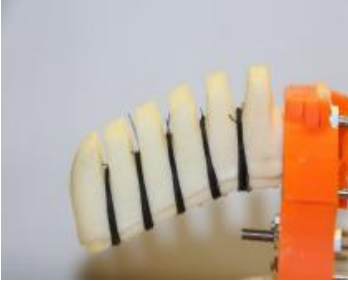
popular actuation system is wire-driven because wire-driven actuation provides more torque and also useful for maintenance. [4,5]. While pneumo actuators demand more design space and difficult maintenance. The latest actuation system is a polymer material called dielectric elastomer. This material can change the size by applying a voltage. despite the material lightness, it requires high voltage, and the mechanical property of the material will decrease after numerous applications.

Many researchers and engineers brought a valuable contribution to the development of continuum robots. In spite of great robot, dexterity features controlling of continuum manipulator is still a seriously challenging issue because of the flexibility of the shape continuum robots suffering lack of payload capacity and provides less accuracy in comparison with traditional rigid link manipulators. The continuum robot history starts from the 1960s when Anderson and Horn presented the first continuum robot arm called Tensor Arm [6]. Furthermore, professor Hirose from the Tokyo Institute of Technology published a first book dedicated to snake-like robots and also proposed motion kinematics [7]. In the late 1990s Jones and Walker presented a novel continuum robot arm named “Elephant trunk,” and then presented a new kinematic solution [18-21].

Moreover, Jones and Walker presented another fluid-driven robot arm called OctArm and also presented a constant curvature kinematic method for soft and fluid-driven robots [14-17]. In the early 2000's UK company OC robotics presented a new continuum arm with tremendous payload capacity and accurate [9]. Moreover, Han Yuan and Zheng li also proposed a kinematic analysis of a continuum robot based on a static model [5, 10-13]. Furthermore, Dong. et. al from Nottingham University proposed continuum robot arm design with twin-pivot compliant joint, which actuated by a cable, and Dong proposed kinematics based on cable length variation [8,22-25].

In this research paper, we consider a discrete hyper-redundant continuum manipulator named TakoBot (Tako means octopus) design, kinematics, and kinetic solutions. Moreover, robot simulation results will demonstrate manipulator potential.

Table 1. Types of continuum manipulators

Discrete hyper-redundant	Hard continuum manipulator	Soft manipulator
		

2. Design concept

2.1 Continuum part design

Due to the robot application, the design could be various. Discrete continuum manipulator structure consists of the following necessary parts: a universal joint, cable routing spacer discs, cables, and helical springs (see fig. 3). The springs had been utilized as joints, such kind of design provides 2DOF bending motion and stiffness to the structure. However, using springs for backbone joints has a drawback, which means the slender part can elongate and shrink, which affects the end-effector position and makes a problematic control process. Moreover, springs consume more power. But there is no other material that can provide such freedom on variable stiffness to the robot slender part, such as springs. To verify this concept, we build two types of continuum manipulators, with a universal joint backbone and with a spring backbone (Fig 2).

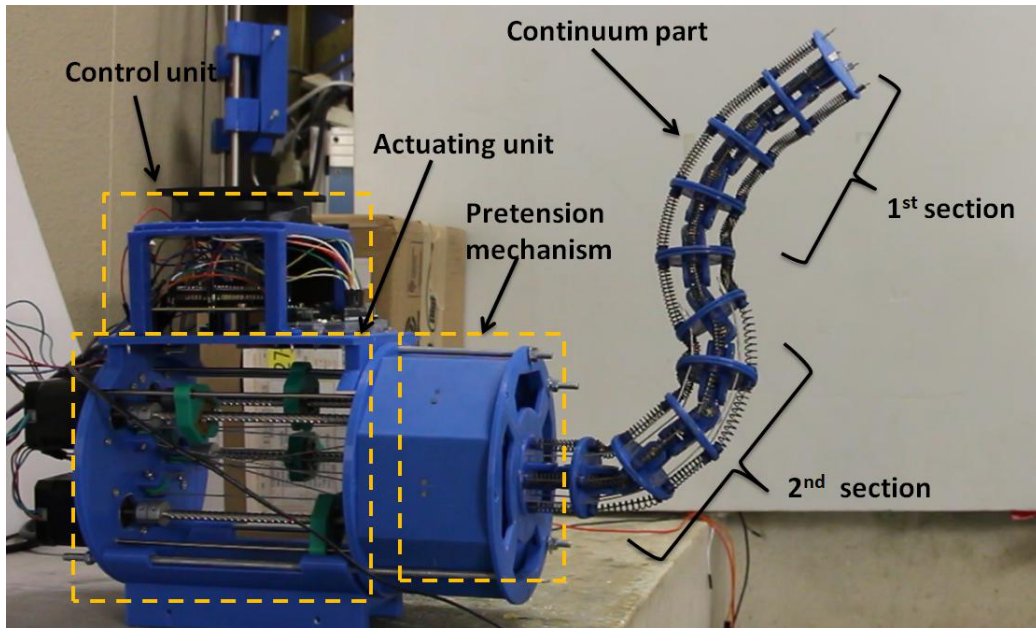
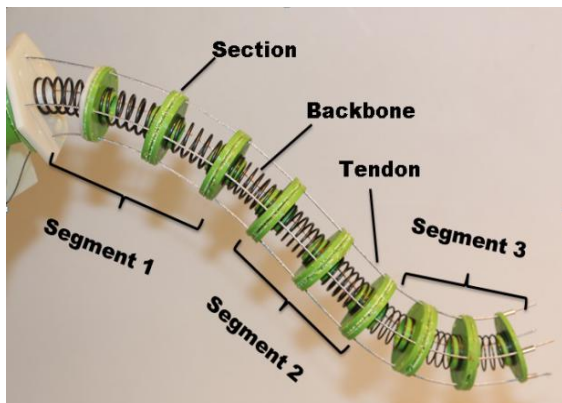
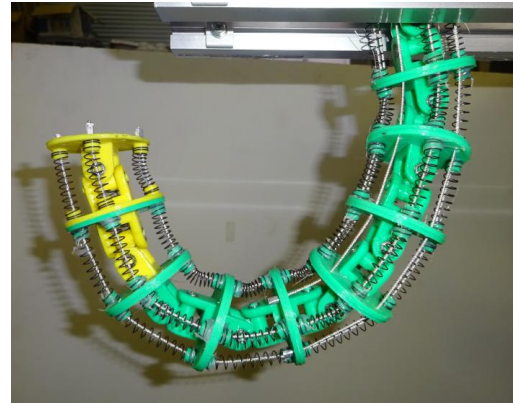


Figure 1. Takobot design



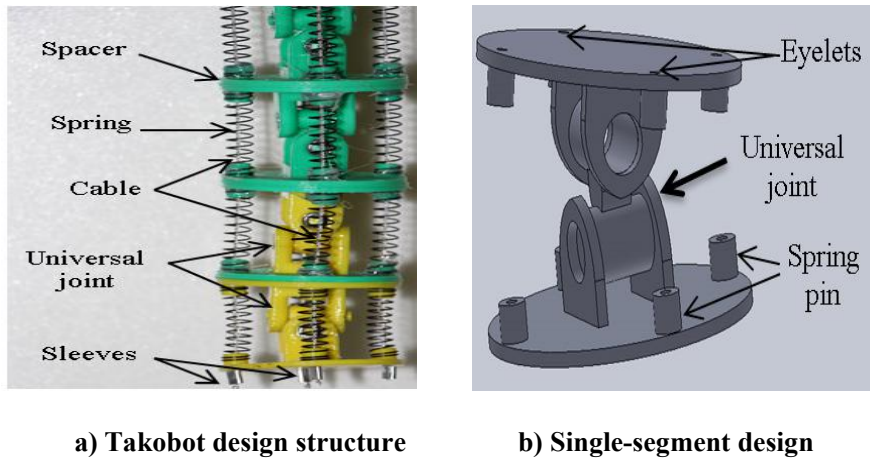
a) Spring backbone



b) Universal joint backbone

Figure 2. Continuum robot design with (a) spring backbone and (b) with a universal joint backbone.

Based on conducted experiments, the spring backboned continuum robot arm has numerous drawbacks with precision and mobile mass [27]. According to the robot design, manipulator could extend and retract, but in a real application, such motion led to inaccuracy, and due to big spring's robot, mobile mass significantly increased. Therefore, to improve robot accuracy, we proposed the next following solutions: each segment should be fixed in length, and mobile mass should be lighter to prevent massive stress to the driving motors [28,29] (Fig.3).



a) Takobot design structure b) Single-segment design

Figure 3. Takobot design structure and single-segment design

The universal joint length could determine the distance between spacer discs, or it should not exceed over 40 mm. Long-distance between two discs might lead to the spring to spring or spring to universal joint interference. Moreover, inner intervention increases friction inside of the structure. Thus, the desired distance is between 30-40 mm per segment. The disc diameter is 50mm and universal joints interconnect spacer discs. Spring pins in figure 3b for fixing the compressional helical springs. The springs had been selected from Misumi manufacturer catalog. In this research, we used spring WF8-40 with spring constant 0.8N/mm, and the deflection rate of the spring is 40%.

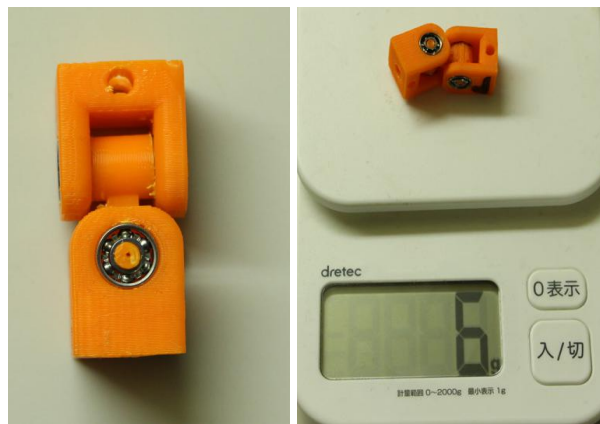


Figure 4. 3d printed universal joint

In this research, we utilized 3d printed universal joint ((Fig. 4). 3d printed universal joint became lighter than commercially available prototypes, and also printed ABS material reliability was acceptable.

2.2 Actuating unit design

There are two types of tendon actuation on continuum manipulators: by a pulley and by a linear shaft. Pulley actuation is a cheaper option, but the main drawback is on the design, which makes difficult motors arrangement. In addition, pulleys cannot generate great torque, which means to achieve enough torque requires big motors, while by linear shaft provides high torque with small motors because of the linear moment and motor locations could be more compact (Fig.5).

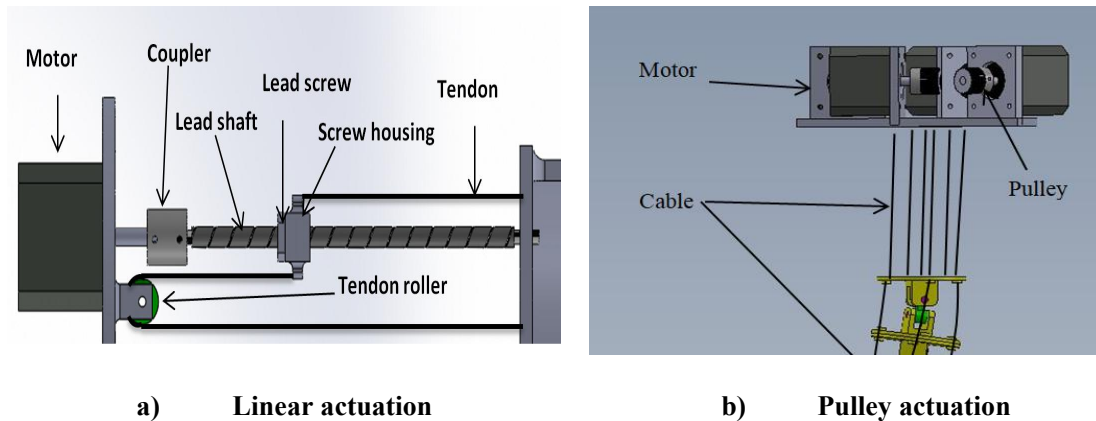


Figure 5. Wire-driven actuating unit types

In the proposed prototype, we used a linear actuating unit with a paired wire driving system. One of the difficulties of the paired wire-driving system is a wire-tension; therefore, such kind of wire-driven system requires a pre-tension mechanism system.

2.3. Pretension mechanism design

Moreover, in wire-driven system design tension issue also should be taking into account as well. In practice, tension control is a quite difficult issue and always tendon slack takes place during the control. Therefore, tendon actuated mechanisms require a pretension mechanism to compensate for lost tension. Our proposed pretension mechanism (PTM) is a passive mechanical device which could be applied almost for all types of actuation.

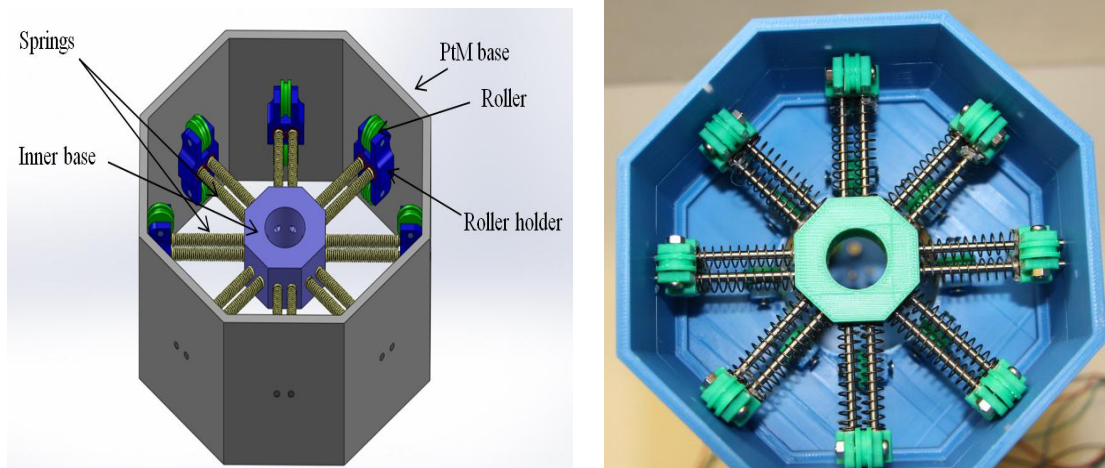


Figure 6. Pretension mechanism CAD design and fabricated prototype

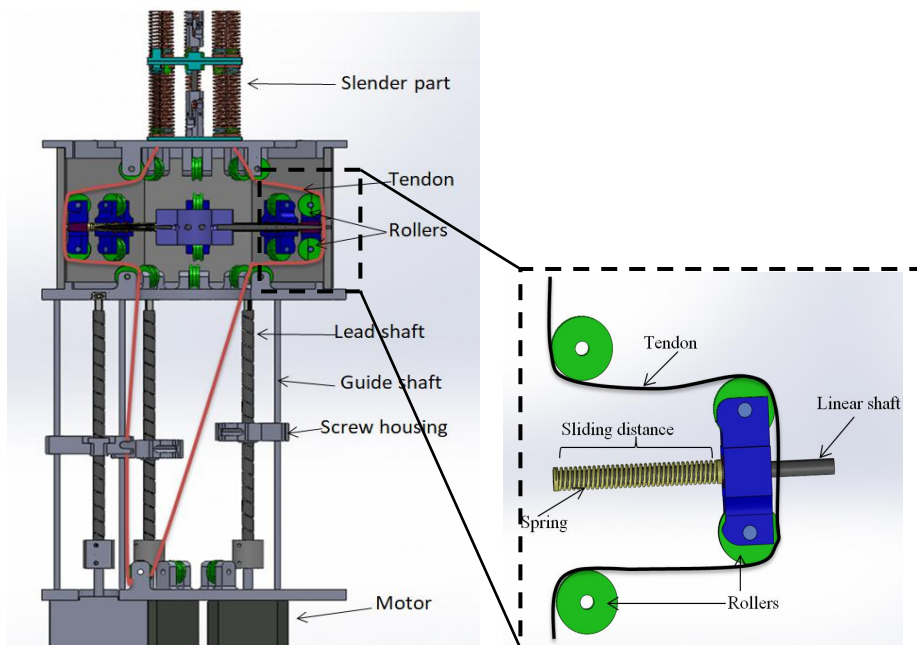


Figure 7. Takobot wire routing schematics

3. Kinematic formulations

3.1. Forward kinematic formulation

Coordinate systems are set at every universal joint.

The homogeneous coordinate transform matrices:

$$\Sigma_0 \rightarrow \Sigma_1: H_{0,1} = \begin{pmatrix} R_y(\theta_{y1})R_x(\theta_{x1}) & \mathbf{u}_{0,1} \\ \mathbf{0} & \mathbf{1} \end{pmatrix}, \mathbf{u}_{0,1} = \begin{pmatrix} x_0 \\ y_0 \\ l_0 \end{pmatrix} \quad (1)$$

$$\Sigma_{i-1} \rightarrow \Sigma_i: H_{i-1,i} = \begin{pmatrix} R_y(\theta_{yi})R_x(\theta_{xi}) & \mathbf{u}_{i-1,i} \\ \mathbf{0} & \mathbf{1} \end{pmatrix}, \mathbf{u}_{i-1,i} = \begin{pmatrix} \mathbf{0} \\ \mathbf{0} \\ L \end{pmatrix}, (i = 2, \dots, n) \quad (2)$$

where, x_0 and y_0 are an initial position of the base. $R_x(\theta_{xi})$ and $R_y(\theta_{yi})$ are rotation matrices of i th universal joint that has two rotation angles θ_{xi} and θ_{yi} , is a rotation matrix of the i th disk with a rotation angle along the axial axis and L is a length between neighboring universal joints (Fig.8). Two rotation matrices have

$$R_x(\theta_{xi}) = \begin{pmatrix} 1 & 0 & 0 \\ 0 & \cos \theta_{xi} & -\sin \theta_{xi} \\ 0 & \sin \theta_{xi} & \cos \theta_{xi} \end{pmatrix}, R_y(\theta_{yi}) = \begin{pmatrix} \cos \theta_{yi} & 0 & \sin \theta_{yi} \\ 0 & 1 & 0 \\ -\sin \theta_{yi} & 0 & \cos \theta_{yi} \end{pmatrix}, \quad (3)$$

Multiplying the H-matrices successively, we get unit vectors and position vector of the i th coordinate system;

where, \mathbf{u}_i is the position of the i th universal joint U_i ($i = 1, \dots, n-1$).

The position vector \mathbf{p}_i of the end-point P_n and position of sliding plates P_i ($i = 1, \dots, n-1$) of the manipulator are obtained by,

$$\begin{pmatrix} \mathbf{p}_i \\ 1 \end{pmatrix} = H_{0,i}(\mathbf{0} \quad \mathbf{0} \quad l_i \quad 1)^T, (i = 1, \dots, n) \quad (4)$$

where, l_n is a fixed length between the n th universal joint and the most distal plate.

Position vectors of 8 hole $A_0, B_0, C_0, D_0, \hat{A}_0, \hat{B}_0, \hat{C}_0, \hat{D}_0$ at the base plate are determined as,

$$\begin{aligned} \mathbf{a}_0 &= \begin{pmatrix} a_x \\ a_y \\ 0 \end{pmatrix}, \mathbf{b}_0 = \begin{pmatrix} b_x \\ b_y \\ 0 \end{pmatrix}, \mathbf{c}_0 = \begin{pmatrix} c_x \\ c_y \\ 0 \end{pmatrix}, \mathbf{d}_0 = \begin{pmatrix} d_x \\ d_y \\ 0 \end{pmatrix}, \\ \hat{\mathbf{a}}_0 &= \begin{pmatrix} \hat{a}_x \\ \hat{a}_y \\ 0 \end{pmatrix}, \hat{\mathbf{b}}_0 = \begin{pmatrix} \hat{b}_x \\ \hat{b}_y \\ 0 \end{pmatrix}, \hat{\mathbf{c}}_0 = \begin{pmatrix} \hat{c}_x \\ \hat{c}_y \\ 0 \end{pmatrix}, \hat{\mathbf{d}}_0 = \begin{pmatrix} \hat{d}_x \\ \hat{d}_y \\ 0 \end{pmatrix}, \end{aligned} \quad (5)$$

Position vectors of 4 hole $A_i, \hat{A}_i, C_i, \hat{C}_i$ at the i th plate ($i = 1, \dots, n$) are obtained as,

$$\begin{pmatrix} \mathbf{a}_i \\ 1 \end{pmatrix} = \mathbf{H}_{0,i} \begin{pmatrix} a_x \\ a_y \\ l_i \\ 1 \end{pmatrix}, \quad \begin{pmatrix} \hat{\mathbf{a}}_i \\ 1 \end{pmatrix} = \mathbf{H}_{0,i} \begin{pmatrix} \hat{a}_x \\ \hat{a}_y \\ l_i \\ 1 \end{pmatrix}, \quad \begin{pmatrix} \mathbf{c}_i \\ 1 \end{pmatrix} = \mathbf{H}_{0,i} \begin{pmatrix} c_x \\ c_y \\ l_i \\ 1 \end{pmatrix}, \quad \begin{pmatrix} \hat{\mathbf{c}}_i \\ 1 \end{pmatrix} = \mathbf{H}_{0,i} \begin{pmatrix} \hat{c}_x \\ \hat{c}_y \\ l_i \\ 1 \end{pmatrix}, \quad (6)$$

$$(i = 1, \dots, n)$$

where, l_i is an axial length between the i th universal joint and the i th plate, which varies as the plate slides along rods, except l_n .

In the same way, position vectors of 4 hole B, $\hat{B}_i, D_i, \hat{D}_i$ at the i th plate ($i = 1, \dots, m$) are obtained as,

$$\begin{pmatrix} \mathbf{b}_i \\ 1 \end{pmatrix} = \mathbf{H}_{0,i} \begin{pmatrix} b_x \\ b_y \\ l_i \\ 1 \end{pmatrix}, \quad \begin{pmatrix} \hat{\mathbf{b}}_i \\ 1 \end{pmatrix} = \mathbf{H}_{0,i} \begin{pmatrix} \hat{b}_x \\ \hat{b}_y \\ l_i \\ 1 \end{pmatrix}, \quad \begin{pmatrix} \mathbf{d}_i \\ 1 \end{pmatrix} = \mathbf{H}_{0,i} \begin{pmatrix} d_x \\ d_y \\ l_i \\ 1 \end{pmatrix}, \quad \begin{pmatrix} \hat{\mathbf{d}}_i \\ 1 \end{pmatrix} = \mathbf{H}_{0,i} \begin{pmatrix} \hat{d}_x \\ \hat{d}_y \\ l_i \\ 1 \end{pmatrix}, \quad (7)$$

$$(i = 1, \dots, m)$$

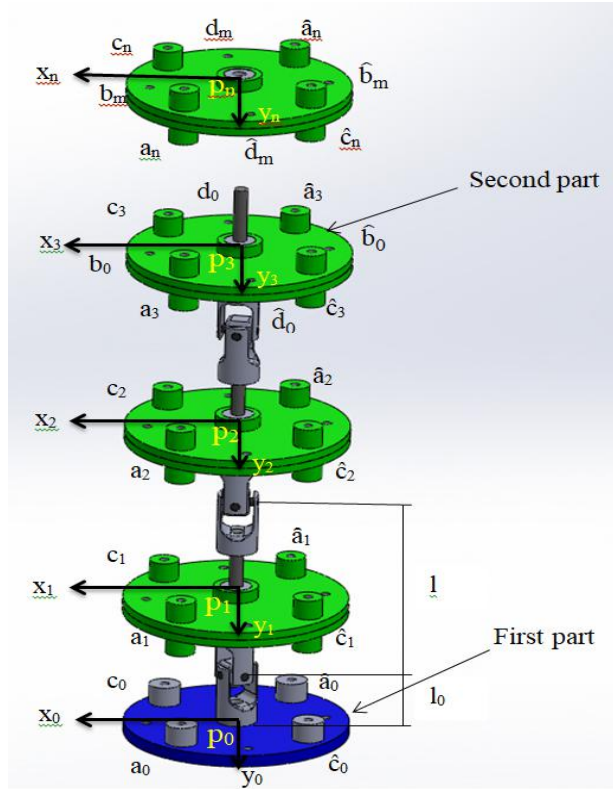


Figure 8. TakoBot Kinematic structure

3.2 Kinetic formulation

Our continuum manipulator is divided into two segments. The first segment is located by the distal part and the second segment is located by the proximal part. The first segment is

operated by 2 pairs of 2 wires; total 4wires. One pair of 2 wires is controlled by one motor that pulls one wire and pushes the other wire in the same length by using the pulley. While, the second segment is operated by 4 pair of 4 wires, total 8 wires. Therefore the second segment is controlled by 4 motors.

The second segment has m units and the first segment has $n-m$ units.

4 pairs of wires are labelled by a and \hat{a} , b and \hat{b} , c and \hat{c} , d and \hat{d} ,

Equilibrium in moments at U_n belonging to the first segment is

$$(S_{a,n} - f_a)(\overline{\mathbf{a}_n - \mathbf{a}_{n-1}}) \times (\mathbf{a}_n - \mathbf{u}_n) + (S_{\hat{a},n} - f_{\hat{a}})(\overline{\hat{\mathbf{a}}_n - \hat{\mathbf{a}}_{n-1}}) \times (\hat{\mathbf{a}}_n - \mathbf{u}_n) + (S_{c,n} - f_c)(\overline{\mathbf{c}_n - \mathbf{c}_{n-1}}) \times (\mathbf{c}_n - \mathbf{u}_n) + (S_{\hat{c},n} - f_{\hat{c}})(\overline{\hat{\mathbf{c}}_n - \hat{\mathbf{c}}_{n-1}}) \times (\hat{\mathbf{c}}_n - \mathbf{u}_n) + m_w(\mathbf{p}_n - \mathbf{u}_n) \times \mathbf{g} = \begin{pmatrix} 0 \\ 0 \\ 0 \end{pmatrix} \quad (8)$$

where, $\overline{\mathbf{a}_n - \mathbf{a}_{n-1}} = \frac{a_n - a_{n-1}}{|a_n - a_{n-1}|}$, etc. m_w is a payload applying at the end-point and \mathbf{g} is the gravity acceleration vector.

Equilibrium in moments at U_i , ($i = m + 1, \dots, n - 1$), belonging to the first segment is

$$\begin{aligned} & \left(-S_{a,i+1}(\overline{\mathbf{a}_{i+1} - \mathbf{a}_i}) + S_{a,i}(\overline{\mathbf{a}_i - \mathbf{a}_{i-1}}) \right) \times (\mathbf{a}_i - \mathbf{u}_i) + \left(-S_{\hat{a},i+1}(\overline{\hat{\mathbf{a}}_{i+1} - \hat{\mathbf{a}}_i}) + S_{\hat{a},i}(\overline{\hat{\mathbf{a}}_i - \hat{\mathbf{a}}_{i-1}}) \right) \times \\ & (\hat{\mathbf{a}}_i - \mathbf{u}_i) + \left(-S_{c,i+1}(\overline{\mathbf{c}_{i+1} - \mathbf{c}_i}) + S_{c,i}(\overline{\mathbf{c}_i - \mathbf{c}_{i-1}}) \right) \times (\mathbf{c}_i - \mathbf{u}_i) + \\ & \left(-S_{\hat{c},i+1}(\overline{\hat{\mathbf{c}}_{i+1} - \hat{\mathbf{c}}_i}) + S_{\hat{c},i}(\overline{\hat{\mathbf{c}}_i - \hat{\mathbf{c}}_{i-1}}) \right) \times (\hat{\mathbf{c}}_i - \mathbf{u}_i) + \left(m_w(\mathbf{p}_n - \mathbf{u}_i) + m_p \sum_{k=i+1}^{n-1} (\mathbf{p}_k - \mathbf{u}_i) \right) \times \mathbf{g} = \begin{pmatrix} 0 \\ 0 \\ 0 \end{pmatrix} \end{aligned} \quad (9)$$

where. $f_a, f_{\hat{a}}, f_c, f_{\hat{c}}$ are wire tensions, $S_{a,i}, S_{\hat{a},i}, S_{c,i}, S_{\hat{c},i}$, ($i = m + 1, \dots, n$) are spring tensions of the i th unit. “ \times ” means a cross product and “ $|\cdot|$ ”, means the modulus of a vector*. m_p is the mass of one unit including the plate, the rod and the universal joint.

The spring tensions are obtained as,

$$\begin{aligned} S_{a,i} &= k(L - |\mathbf{a}_i - \mathbf{a}_{i-1}|), S_{\hat{a},i} = k(L - |\hat{\mathbf{a}}_i - \hat{\mathbf{a}}_{i-1}|), \\ S_{c,i} &= k(L - |\mathbf{c}_i - \mathbf{c}_{i-1}|), S_{\hat{c},i} = k(L - |\hat{\mathbf{c}}_i - \hat{\mathbf{c}}_{i-1}|), \end{aligned} \quad (10)$$

with spring coefficient k . Equations (8) and (9) contain $3(n-m)$ equations including $4(n-m)$ - 1 variables of the $n-m$ universal joints angles $\theta_{xi}, \theta_{yi}, \theta_{zi}$, ($i = m + 1, \dots, n$) and slide length of plates l_i ($i = m + 1, \dots, n - 1$).

Equilibrium in force at the i th plate ($i = m + 1, \dots, n - 1$) is,

$$\begin{aligned} & \left(-S_{a,i+1}(\overline{\mathbf{a}_{i+1} - \mathbf{a}_i}) + S_{a,i}(\overline{\mathbf{a}_i - \mathbf{a}_{i-1}}) - S_{\hat{a},i+1}(\overline{\hat{\mathbf{a}}_{i+1} - \hat{\mathbf{a}}_i}) + S_{\hat{a},i}(\overline{\hat{\mathbf{a}}_i - \hat{\mathbf{a}}_{i-1}}) - S_{c,i+1}(\overline{\mathbf{c}_{i+1} - \mathbf{c}_i}) + \right. \\ & \left. S_{c,i}(\overline{\mathbf{c}_i - \mathbf{c}_{i-1}}) - S_{\hat{c},i+1}(\overline{\hat{\mathbf{c}}_{i+1} - \hat{\mathbf{c}}_i}) + S_{\hat{c},i}(\overline{\hat{\mathbf{c}}_i - \hat{\mathbf{c}}_{i-1}}) + (n - i)m_p \mathbf{g} \right) \cdot (\mathbf{p}_i - \mathbf{u}_i) = 0 \end{aligned} \quad (11)$$

(11) provide $n-m-1$ equations. Combined it with (8) and (9), we obtain $4(n-m)-1$ equations, which suffices in number to solve for $4(n-m)-1$ variables; $\theta_{x,i}, \theta_{y,i}, \theta_{z,i}$ ($i = m+1, \dots, n$) and l_i ($i = m+1, \dots, n-1$) for a given set of wire tensions $f_a, f_{\hat{a}}, f_c, f_{\hat{c}}$.

Equilibrium in moments at U_m , the universal joint located at the most distal position belonging to the second segment is

$$\begin{aligned}
& -S_{a,m+1}(\overline{\mathbf{a}_{m+1} - \mathbf{a}_m}) \times (\mathbf{a}_m - \mathbf{u}_m) + (S_{b,m} - f_b)(\overline{\mathbf{b}_m - \mathbf{b}_{m-1}}) \times (\mathbf{b}_m - \mathbf{u}_m) \\
& -S_{\hat{a},m+1}(\overline{\hat{\mathbf{a}}_{m+1} - \hat{\mathbf{a}}_m}) \times (\hat{\mathbf{a}}_m - \mathbf{u}_m) + (S_{\hat{b},m} - f_{\hat{b}})(\overline{\hat{\mathbf{b}}_m - \hat{\mathbf{b}}_{m-1}}) \times (\hat{\mathbf{b}}_m - \mathbf{u}_m) \\
& -S_{c,m+1}(\overline{\mathbf{c}_{m+1} - \mathbf{c}_m}) \times (\mathbf{c}_m - \mathbf{u}_m) + (S_{d,m} - f_d)(\overline{\mathbf{d}_m - \mathbf{d}_{m-1}}) \times (\mathbf{d}_m - \mathbf{u}_m) \\
& -S_{\hat{c},m+1}(\overline{\hat{\mathbf{c}}_{m+1} - \hat{\mathbf{c}}_m}) \times (\hat{\mathbf{c}}_m - \mathbf{u}_m) + (S_{\hat{d},m} - f_{\hat{d}})(\overline{\hat{\mathbf{d}}_m - \hat{\mathbf{d}}_{m-1}}) \times (\hat{\mathbf{d}}_m - \mathbf{u}_m) \\
& + \left(m_w(\mathbf{p}_n - \mathbf{u}_m) + m_p \sum_{k=m+1}^{n-1} (\mathbf{p}_k - \mathbf{u}_m) \right) \times \mathbf{g} = \begin{pmatrix} 0 \\ 0 \\ 0 \end{pmatrix}
\end{aligned} \tag{12}$$

For the second segment, we can derive the similar equations as (9), (10) and (11) by replacing $\{\mathbf{a}_i, \hat{\mathbf{a}}_i, \mathbf{c}_i, \hat{\mathbf{c}}_i\}$ with $\{\mathbf{b}_i, \hat{\mathbf{b}}_i, \mathbf{d}_i, \hat{\mathbf{d}}_i\}$, $\{S_{a,i}, S_{\hat{a},i}, S_{c,i}, S_{\hat{c},i}\}$ with $\{S_{b,i}, S_{\hat{b},i}, S_{d,i}, S_{\hat{d},i}\}$ for $i = 1, \dots, m-1$ in (10) and for $i = 1, \dots, m$ in (10) and (11).

As a result, we obtain $4m$ equations included by (12), which suffices in number to solve for $4m$ variables; $\theta_{x,i}, \theta_{y,i}, \theta_{z,i}$ and l_i ($i = 1, \dots, m$) for a given set of wire tensions $f_b, f_{\hat{b}}, f_d, f_{\hat{d}}$.

Wire tensions $f_a, f_{\hat{a}}, f_c, f_{\hat{c}}, f_b, f_{\hat{b}}, f_d, f_{\hat{d}}$ are determined according to 4 motors' angles $\phi_a, \phi_b, \phi_c, \phi_d$

as,

$$\begin{aligned}
f_a &= k_p \left(\frac{\lambda(\phi_p + \phi_a)}{2\pi} - nL + \sum_{i=1}^n |\mathbf{a}_i - \mathbf{a}_{i-1}| \right), \quad f_{\hat{a}} = k_p \left(\frac{\lambda(\phi_p - \phi_a)}{2\pi} - nL + \sum_{i=1}^n |\hat{\mathbf{a}}_i - \hat{\mathbf{a}}_{i-1}| \right), \\
f_c &= k_p \left(\frac{\lambda(\phi_p + \phi_c)}{2\pi} - nL + \sum_{i=1}^n |\mathbf{c}_i - \mathbf{c}_{i-1}| \right), \quad f_{\hat{c}} = k_p \left(\frac{\lambda(\phi_p - \phi_c)}{2\pi} - nL + \sum_{i=1}^n |\hat{\mathbf{c}}_i - \hat{\mathbf{c}}_{i-1}| \right), \\
f_b &= k_p \left(\frac{\lambda(\phi_p + \phi_b)}{2\pi} - nL + \sum_{i=1}^m |\mathbf{b}_i - \mathbf{b}_{i-1}| \right), \quad f_{\hat{b}} = k_p \left(\frac{\lambda(\phi_p - \phi_b)}{2\pi} - nL + \sum_{i=1}^m |\hat{\mathbf{b}}_i - \hat{\mathbf{b}}_{i-1}| \right), \\
f_d &= k_p \left(\frac{\lambda(\phi_p + \phi_d)}{2\pi} - nL + \sum_{i=1}^m |\mathbf{d}_i - \mathbf{d}_{i-1}| \right), \quad f_{\hat{d}} = k_p \left(\frac{\lambda(\phi_p - \phi_d)}{2\pi} - nL + \sum_{i=1}^m |\hat{\mathbf{d}}_i - \hat{\mathbf{d}}_{i-1}| \right)
\end{aligned} \tag{13}$$

where, ϕ_p is a motor rotation angle to generate a pretension, λ is a lead of the screw rod and k_p is the spring constant of the pretension spring.

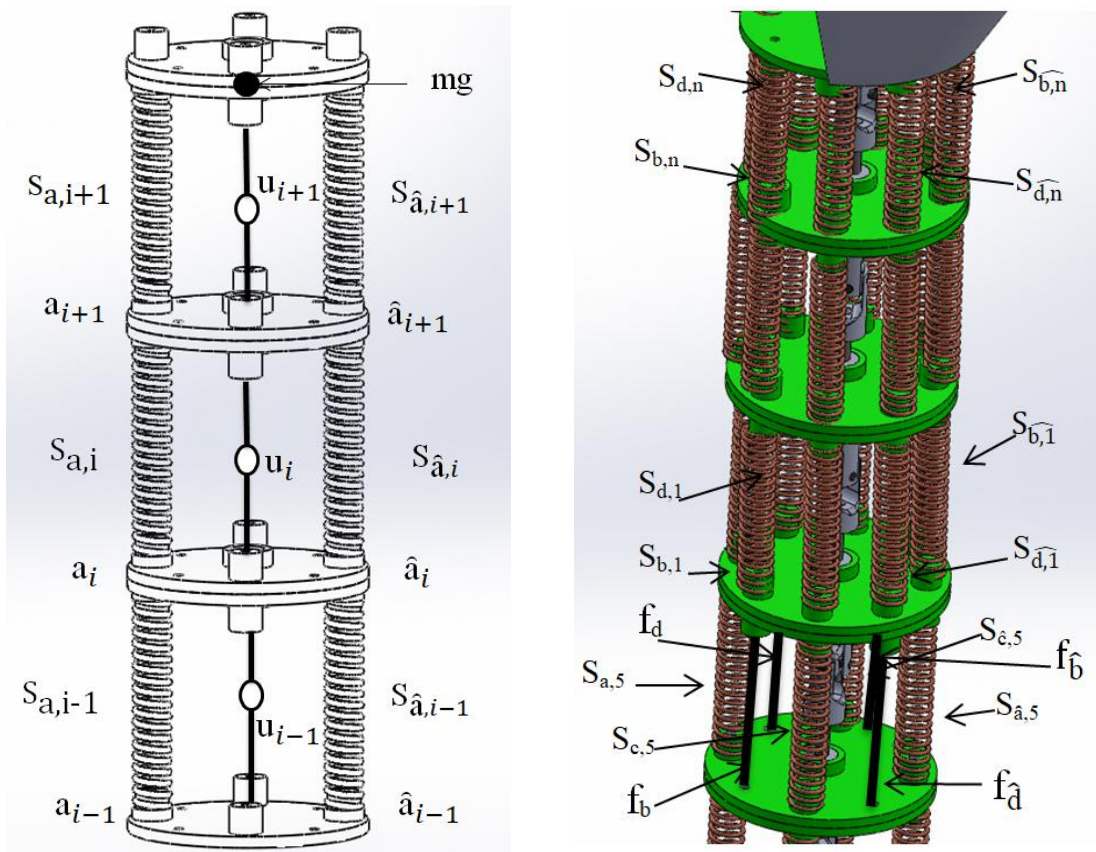


Figure 9. Takobot kinetic structure.

4. Robot control

The proposed manipulator control is the teleoperated method. In this research, we used two joysticks. According to the robot design, the manipulator in total has four motors; two motors for end-effector and the other two for the mid-section. Each manipulator has two degrees of freedom, and in actuation, it notes as x and y-axis. As an actuating unit, we used bipolar stepping motors with 0.69Nm torque. The motor driver is TMC 2208 from (Trinamic Motion INC). The controller is Arduino UNO.

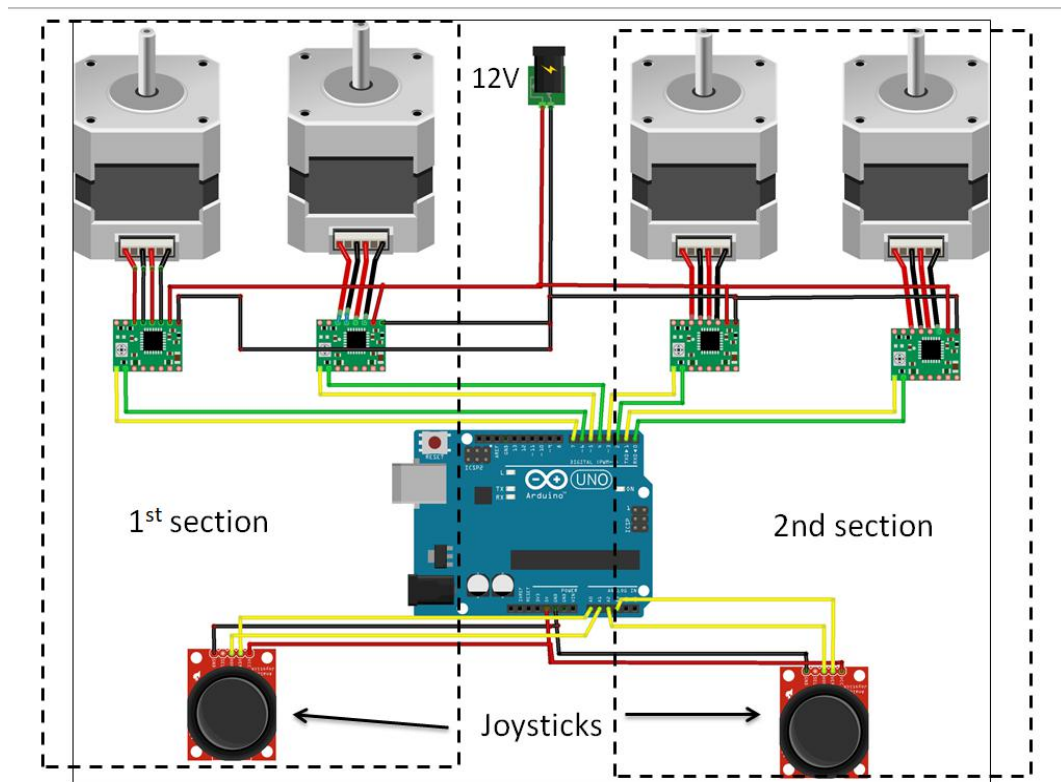


Figure 10. Takobot control schematics

Figure 10 shows that control schematics and control board wiring. The control board power supply is variable, motor drivers and stepping motors consume 12V, Arduino board and joysticks consumes only six voltages. For the continuous work, we included a cooler fan additionally.

Motion starts from the joysticks; it gives the desired driving direction to the motors. In general, the robot can move in four directions: up, down, left, and right. Those primitive motions which are enough to reach the desired position. Due to 2 actuated sections, based on robot wire arrangement design, it makes the control process complicated. The first section wires located with the 90-degree arrangement, same as x and y –axes, but the second section wires aligned in 45 degrees, which means co-directional motions of first and second sections should be coherent. Otherwise, control would be very complicated. Moreover, both sections cannot be controlled with a single joystick because to improve the reachability of the manipulator robot should do ‘S’ shape motions, which is possible only with two joysticks control.

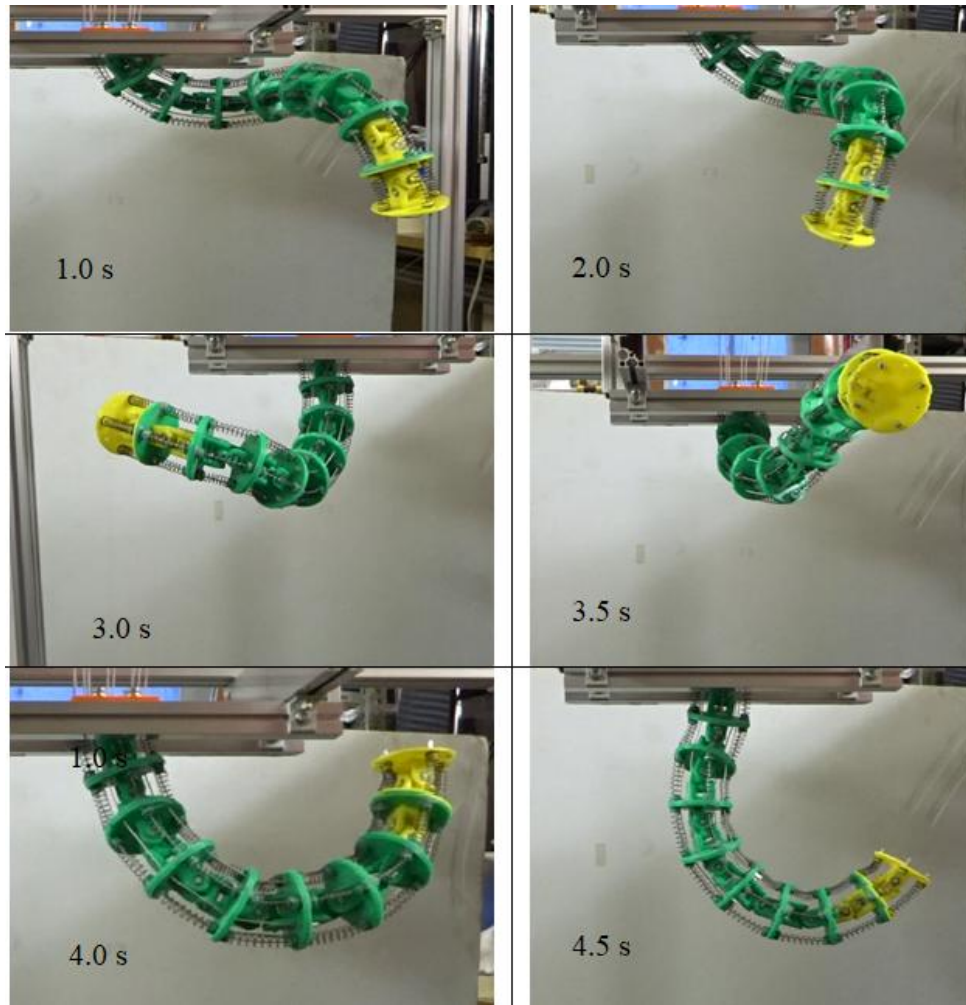


Figure 13. Basic manipulation experiments

Conclusion

In this research, we developed a 3dprinted wire-driven continuum robot arm.

Moreover, the research described the robot design, kinematics, and control strategy of the proposed manipulator. According to the conducted experiments, we could determine the optimal size of the robot segment and analyzed the robot backbone design. The proposed design demonstrated better accuracy and smooth motion. Based on observation, using springs in the segment provided rigidity and depends on the required stiffness, we could increase spring constants by replacing them. Compare with other materials, and only spring can give such freedom on selecting required hardness.

In the near future, we are planning to improve robot payload capacity and find a proper application.

Acknowledgments

A.Y. admires his gratitude to Satbayev University for Ph.D. funding.

References

- [1] D.Caleb Rucker, Robert J Webster III., Statics and Dynamics of Continuum Robots With General Tendon Routing and External Loading, IEEE TRANSACTIONS ON ROBOTICS, vol.27.NO.6.December 2011
- [2] Guochen Niu, Li Wang and Guanghua Zong, Attitude control based on fuzzy logic for continuum aircraft fuel tank inspection robot, 29 (2015)
- [3] Zheng li, Liao Wu, Hongliang Ren, Haoyong Yu, Kinematic comparison of surgical tendon-driven manipulators and concentric tube manipulators, Machine and Mechanism, 148-165 pp, (2017)
- [4] Kun Cao, et.al. Workspace Analysis of tendon –driven Continuum Robots Based on Mechanical Interference Identification, Journal of Mechanical Design, 2017.
- [5] Zheng Li and Ruxu Du, Design and Analysis of a Bio-inspired Wire-Driven Multi-Section Flexible Robot, International Journal of Advanced Robotic Systems, 2013.
- [6] Anderson, V.C.; Horn, R.C. Tensor arm manipulator design. Trans. ASME 1967, 67, 1–12.
- [7] Aoki, T.; Ochiai, A.; Hirose, S. Study on slime robot development of the mobile robot prototype model using bridle bellows. In Proceedings of the IEEE International Conference on Robotics and Automation, New Orleans, LA, USA, 26 April–1 May 2004; pp. 2808–2813.
- [8] Xin Dong, and et.al, A Novel Continuum Robot Using Twin-Pivot Compliant Joints: Design, Modelling, and Validation., Journal of Mechanisms and Robotics, 2016.
- [9] Rob Buckingham, Andrew Graham, (2012) "Nuclear snake-arm robots", Industrial Robot: An International Journal ,Vol. 39 Issue:1 pp. 6-11, <https://doi.org/10.1108/01439911211192448>
- [10] K. Suzumori, S. Iikura and H. Tanaka, Development of Flexible Microactuator and Its Applications to Robotic Mechanisms}, pp. 1622-1627, Proceedings of the 1991 IEEE International Conference on Robotics and Automation, Sacramento, California, 1991.
- [11] Michael W. Hannan and Ian D. Walker, Kinematics and the Implementation of an Elephant's Trunk Manipulator and Other Continuum Style Robots, Journal of Field Robotics, volume 20, Issue 2, pp 45-63, <https://doi.org/10.1002/rob.10070>

- [12] M.D. Grissom, I.D. Walker, Design and experimental testing of the OctArm soft robot manipulator, Proc. Of SPIE, 2006.
- [13] W. McMahan, I.D. Walker field Trials and Testing of the OctArm Continuum Manipulators, pp. 2336-2341, Proceedings of 2006 IEEE International Conference on Robotics and Automation, Orlando, Florida, 2006.
- [14] P.E. Dupont, J. Lock, B. Itkowitz and E. Butler, Design and Control of Concentric-Tube robots, Vol.26, No.2, pp. 209-225, IEEE Trans. Robotics., 2010.
- [15] P. Sears and P.E. Dupont, Inverse Kinematics of Concentric Tube Steerable needles, pp. 1887-1892, IEEE International Conference on Robotics and Automation, Roma, Italy, April 2007.
- [16] L.A. Lyons, R. J. Webster III and R. Alterovitz, Motion planning for active Cannulas, pp.801-806, IEEE/RSJ International Conference on Intelligent Robots and Systems (IROS), Oct. 2009.
- [17] D.C. Rucker, B.A. Jones and R.J. Webster III, A geometrically Exact Model for Externally Loaded Concentric-Tube Continuum Robots, Vol.26, №5, IEEE Transactions on Robotics, Oct2010.
- [18] R.H. Sturges, S. Laowattana, A flexible tendon controlled device for endoscopy, pp 2582-2591, Proceedings of the 1991 IEEE International Conference and Automation, Sacramento, California, April, 1991.
- [19] Bo Ouyang, Yunhui Liu and Dong Sun Design Shape Control of a Three-section Continuum Robot, pp. 1151-1156, Proceeding of the 2016 IEEE International Conference on Advanced Intelligent Mechatronics, Banff, Alberta, Canada, July 12-15, 2016
- [20] R.J. Webster and B.A. Jones, Design and kinematics of modelling constant curvature continuum Robots, IntJ Robot.Res., vol29,pp. 1661-1683,2010
- [21] B.A. Jones and I.D. Walker, Kinematics for multisection continuum robots, IEEE TransRobotics, vol 43-55,2006
- [22] B.A. Jones and I.D. Walker, Practical kinematics for real-time implementation continuum robots, IEEE TransRobotics, vol 22, pp 1087-1099, 2006
- [23] J. Burgner, D.C. Rucker, H.B. Gilbert, P.J. Swaney, P.T. Russel, K.D. Weaver at.all, A telerobotic system for transnasal surgery, IEEE/ASME Trans. Mechatronics, vol 19, 996-1006, 2014
- [24] D. Trivedi, A. Lotfi, and C.D. Rahn, Geometrically exact module for soft robotic manipulators, IEEE TransRobot, vol24, pp 773-780, 2008.

- [25] D.C. Rucker, B.A. Jones, R.S. Webster, A geometrically exact model for externally loaded concentric-tube continuum robots, *IEEE TransRobot*, vol 26, pp 769-780, 2010.
- [26] D.B. Camarillo, C.F. Milne, C.R. Carlson, M.R. Zinn, and J.K. Salisbury, Mechanics modelling of tendon –driven continuum manipulators, *IEEE TransRobot*, vol 24, pp 1262-1273, 2008.
- [27] A. Yeshmukhametov, Z. Buribayev, Y. Amirgaliyev and R. Ramakrishanan. “Modeling and Validation of New Continuum Robot Backbone Design With Variable Stiffness Inspired from Elephant Trunk” IOP conference series on material science and engineering, ICMMR 2018, Tokyo, July, 2018.
- [28] A. Yeshmukhametov, K. Koganezawa and Y. Yamamoto, “A Novel Discrete Wire-Driven Continuum Robot Arm with Passive Sliding Disc: Design, Kinematics and Passive Tension Control”, *Robotics Journal*, MDPI, July 2019
- [29] A. Yeshmukhametov, K. Koganezawa and Y. Yamamoto, “Design and Kinematics of Cable-Driven Continuum Robot Arm with Universal Joint Backbone”, *IEEE International Conference on Robotics and Biomimetics*, December, Kuala-Lumpur, 2018